

Crossing the capacity threshold in Si-S batteries through mud-crack electrodes

Zhaotian Xie^{a,b,1}, Wentao Zhang^{a,b,1}, Xin He^{a,b}, Ziyao Gao^{a,b}, Zhicheng Du^c, Hongkai Yang^d, Xinming Zhang^{a,b}, Rui li^{a,b}, Yanbing He^a, Lele Peng^{a,*}, Feiyu Kang^{a,b,*}

^a Institute of Materials Research, Tsinghua Shenzhen International Graduate School, Tsinghua University, Shenzhen 518055, China

^b School of Materials Science and Engineering, Tsinghua University, Beijing 100084, China

^c Institute of Biopharmaceutics and Health Engineering, Tsinghua Shenzhen International Graduate School, Shenzhen 518055, China

^d School of Advanced Materials, Shenzhen Graduate School, Peking University, Shenzhen 518055, China

ARTICLE INFO

Keywords:

Si-S battery
Li-S battery
Capacity threshold
Mud-crack structured Si anode
Lithium-ion diffusion

ABSTRACT

Silicon-Sulfur (Si-S) battery may promise high energy density and stability thanks to the high-capacity and less-dendrite-formation features of Si anode. However, current design principle for Si-S battery relies on a lab-scale, trial-and-error approach to designing and pairing sophisticated sulfur cathodes and Si/C anodes, lacking a feasible protocol to achieve practical application. Herein, we reveal that the Si-S battery made with commercially available Si/C and sulfur will reach a capacity (discharge) threshold that is independent of the mass of sulfur. This phenomenon is caused by the extremely sluggish Li⁺ diffusion at the charging plateaus (~0.43 V) of silicon. In response to this challenge, we propose a dry-slurry process to fabricate a mud-crack structured Si electrode with significantly improved Li⁺ diffusion behavior, which could fully release the capacity of the full cell at low NP ratio by surpassing the capacity threshold. The resulting Si-S battery delivers a specific capacity of 1086 mAh g⁻¹ and 9.7 mAh cm⁻² with a sulfur loading of 8.9 mg cm⁻², which is much higher than the device based on the conventionally made Si/C electrode. Furthermore, the corresponding Si-S pouch cell achieves ~600 mAh g⁻¹ after 200 cycles, showing a better stability compared to Li-S battery at a practical level. These findings suggest that charge transfer in the anode plays a decisive role in the overall performance and provides an overarching design protocol for fabricating practical Si-S full batteries.

1. Introduction

Lithium-sulfur (Li-S) battery has been emerging as an important energy storage technology to tackle the energy and environmental crisis because of its high theoretical energy density, low cost and environmental friendliness [1–5]. Thanks to the two-electron redox reaction between the sulfur and lithium, Li-S battery delivers a high theoretical energy density of 2600 Wh kg⁻¹ which is 3 times higher than that of the layered oxide cathode system [6–12], making it a promising candidate to the existing auto battery. However, the conventional Li-S battery faces critical challenges that hinder its successful implementation in practical applications. One major challenge is that the insulating nature of sulfur and the discharging products leads to the sluggish reaction kinetics and a high activation energy for polysulfide conversion, which fundamentally results in the polysulfide shuttling effect [13–15]. Such

charge transfer issue becomes more problematic in practical Li-S battery devices, where high sulfur loading and mass are always required to achieve high energy. Another major challenge lies in the lithium anode, which suffers from dendrite formation and high reactivity with the soluble polysulfides, causing safety risk and serious capacity decay [16]. Although the overall electrochemical performance of the state-of-the-art Li-S battery has been improved to a very high level through various strategies, such as sulfur catalysis, lithium stabilization and electrolyte engineering, these efforts have majorly been for demonstration purpose on lab-scale coin cell devices and none have been successfully commercialized [17–19]. In this regard, developing an alternative sulfur-based battery that can maintain the unique features of sulfur cathode while avoiding the critical challenges from lithium represents a promising solution to this dilemma.

Applying silicon/carbon (Si/C) anode to replace lithium in Li-S

* Corresponding authors at: Institute of Materials Research, Tsinghua Shenzhen International Graduate School, Tsinghua University, Shenzhen 518055, China.

E-mail addresses: penglele@sz.tsinghua.edu.cn (L. Peng), fykang@mail.tsinghua.edu.cn (F. Kang).

¹ These authors contributed equally to this work.

chemistry has gained considerable interests owing to the tremendous analogies between Si and Li, such as high theoretical specific capacity (4200 mAh g^{-1}) and low discharge voltage ($0.2\text{--}0.4 \text{ V}$ vs Li/Li^+) [20–22]. More importantly, Si-S electrochemistry provides an effective solution to address the cycling performance issue of traditional Li-S battery because of the low-dendrite feature of Si anode. During the electroplating process in lithium anode, the development of a cation concentration gradient between the cathode and anode leads to the formation of a local space charge, which consequently induces dendritic depositions [23]. Different from direct plating and stripping, lithium ions are alloying elements into the silicon lattice in the silicon anode. This mechanism can reduce lithium-ion accumulation in the charging state, thereby reducing the concentration and potential gradient effects [24]. Therefore, silicon and the lithiated silicon could restrain the lithium dendrite formation on their surfaces, which fundamentally resolve the cyclability and safety issues brought by the lithium dendrites. Up to date, most studies have been primarily centered on the design and optimal pairing of sulfur cathode and Si/C anode materials, aiming to validate the practicality of Si-S full cells [25–29]. For example, sophisticated sulfur cathodes and/or silicon anodes have been designed to demonstrate how structural design can enhance the electrochemical performance of the full cell. Pomegranate-structured electrode materials were designed to improve the rate and cycling performance because the pomegranate-like carbon shell could buffer the volume expansion of both electrodes and promote polysulfide conversion in the sulfur cathode side [30]. Loading silicon and sulfur separately into a porous carbon matrix to make carbonaceous composite electrodes is also applied to improve the overall performance of full battery. The full battery consisted of a nano-silicon@carbon nanofiber anode and a sulfur@heteroatom doped carbon cathode, showed an initial capacity of 972 mAh g^{-1} and 50 % capacity retention after 100 cycles [31]. However, current research on Si-S battery is still in its infant stage, and the aforementioned trial-and-error research efforts focus only on devices with limited sulfur loading (typically $\sim 1 \text{ mg cm}^{-2}$), which contradicts the high-energy-density characteristics of the Si-S battery. To the best of our knowledge, none of these efforts have ever touched upon the requirements of making the Si-S battery into practical applications, let alone the commercialization of such battery [32]. Referencing the commercialization standards of current Li-ion batteries, the future commercialization of sulfur-based battery should also be based on electrode materials that are easily accessible, cost-effective and ultra-stable in air. This also emphasizes the high feasibility of replacing lithium with silicon, thanks to its large natural abundance (28 %) and good chemical stability. However, the synthesis of the sophisticated sulfur cathodes and/or silicon anodes requires complicated procedures, introducing additional difficulties to the large-scale production of such materials. Therefore, developing a comprehensive design principle regarding the electrode structure and key parameters based on commercialized anodes and cathodes that affect the overall performance of the full device remains critically challenging and elusive.

In this work, we reveal that the Si-S battery made with a commercial Si/C anode and a sulfur cathode will reach a capacity (discharge) threshold that is independent of the mass of the cathode. GITT results identify that this phenomenon is attributed to the extremely sluggish Li^+ diffusion at the charging plateaus ($\sim 0.43 \text{ V}$) of Si/C anode. To this end, we propose a dry-slurry process protocol to fabricate the Si/C anode (denoted as DS-Si), featuring a mud-crack electrode structure and high packing density that enables superior Li^+ conduction behavior. The resulting Si/C anode displays a much-improved Li^+ diffusion coefficient (particularly at the 0.43 V charging region) than that of the conventional slurry-made anode (denoted as CS-Si). Furthermore, we revealed that the ability to surpass the capacity threshold at low NP ratio plays a decisive role in fully releasing the full cell capacity. Under a 1.2 NP ratio, Si-S full cell devices with DS-Si and CS-Si exhibit a significant difference in their initial capacities, with the former crossing the threshold displaying 1073 mAh g^{-1} (4.0 mAh cm^{-2}), while the latter showing 657 mAh g^{-1} (2.4 mAh cm^{-2}). Based on the mud crack Si anode, the high loading

Si-S full cell could reach 9.7 mAh cm^{-2} with 1086 mAh g^{-1} . Additionally, we also demonstrate that the strategy of crossing the capacity threshold represents a promising protocol toward the practical development of Si-S battery, and the resulting Si-S pouch cell achieves better cycling stability than the Li-S pouch cell, maintaining 690 mAh g^{-1} after 100 cycles. These findings suggest that charge transfer in anode plays a critical role in determining overall performance and provide a key design principle for fabricating practical Si-S full cells.

2. Results

2.1. Intrinsic origin of the capacity threshold in Si-S battery

The Si-S battery offers a high theoretical energy density (1730 Wh kg^{-1} , based on Li_2S and silicon) and improved safety performance compared to the traditional Li-S battery. To achieve a high-energy-density sulfur-based battery, “five 5s” metrics were proposed as essential for meeting the high-energy target [33]. According to a theoretical simulation (Fig. S1), when the sulfur loading is between 1 and 5 mg cm^{-2} , the energy density of the Si-S battery significantly increases as the sulfur loading rises. Once the sulfur loading reaches a certain value, further increases do not significantly impact the energy density. Therefore, developing a comprehensive design principle regarding the electrode structures and key parameters that affect the overall performance of the full device remains critically urgent.

Increasing the mass loading (typically $> 5 \text{ mg cm}^{-2}$) of the active materials in the electrode represents a straightforward strategy to improve energy density, particularly in the lithium-sulfur battery system⁹. Starting with Li-S half cells, composite sulfur electrodes with mass loading of 2.8, 4.3 and 6.4 mg cm^{-2} were fabricated and paired with the Li metal anodes. Surprisingly, a high specific capacity of 1143 mAh g^{-1} was achieved in the sulfur electrode with 6.4 mg cm^{-2} , which is slightly lower than that of the sulfur electrode with 2.8 mg cm^{-2} (Fig. 1a, top). This mass-independent specific capacity performance was attributed to a low current density (0.05 C) and the 3D current collector, which ensures good charge transfer. While the capacities (discharges) delivered by the three sulfur cathodes were proportional to the mass loading of the sulfur, i.e. sulfur cathodes with the loading of 6.4 mg cm^{-2} delivered the largest charge of 7.3 mAh and the 2.8 mg cm^{-2} sulfur electrode delivered 3.3 mAh. When the same cathodes were paired with Si/C anodes with the same loading, representing the similar charges or lithium amounts (with values of 5.31 mAh, 5.91 mAh and 5.43 mAh, respectively, as shown in the prelithiation curves on the lower side of Fig. 1b), the specific capacities of those Si-S full batteries showed dramatically different values, with the trend that higher mass loading resulted in lower specific capacity (Fig. 1a, bottom). However, the discharge capacities (or charges delivered) of the three full cells were surprisingly aligned even when the discharge voltage were reduced from 0.8 V to 0.4 V. The capacities were measured at 2.73 mAh, 2.97 mAh and 2.85 mAh, respectively (Fig. 1b). When the discharge curves of the Si-S batteries were mapped onto the charge curves of the silicon anodes for better comparison, it was found that the charges (or lithium amounts) stored in the sulfur electrodes with different loadings corresponded well with the lithiation amount at the charging plateau of the Si/C anodes, which corresponded to a voltage of approximately 0.43 V. It seemed that a threshold existed at 0.43 V in the silicon anode, which hindered the release of capacity throughout the full cell. In other words, the additional capacity on the silicon anode could not be further utilized when the voltage exceeded 0.43 V.

To confirm our hypothesis, the galvanostatic intermittent titration technique (GITT) was utilized to evaluate the lithium-diffusion performance of the anodes. To eliminate the influence of surface roughness, copper foils were used as current collectors. The diffusivity of Li^+ can be analyzed in accordance with Fick's second law, as outlined in the simplified Equation.

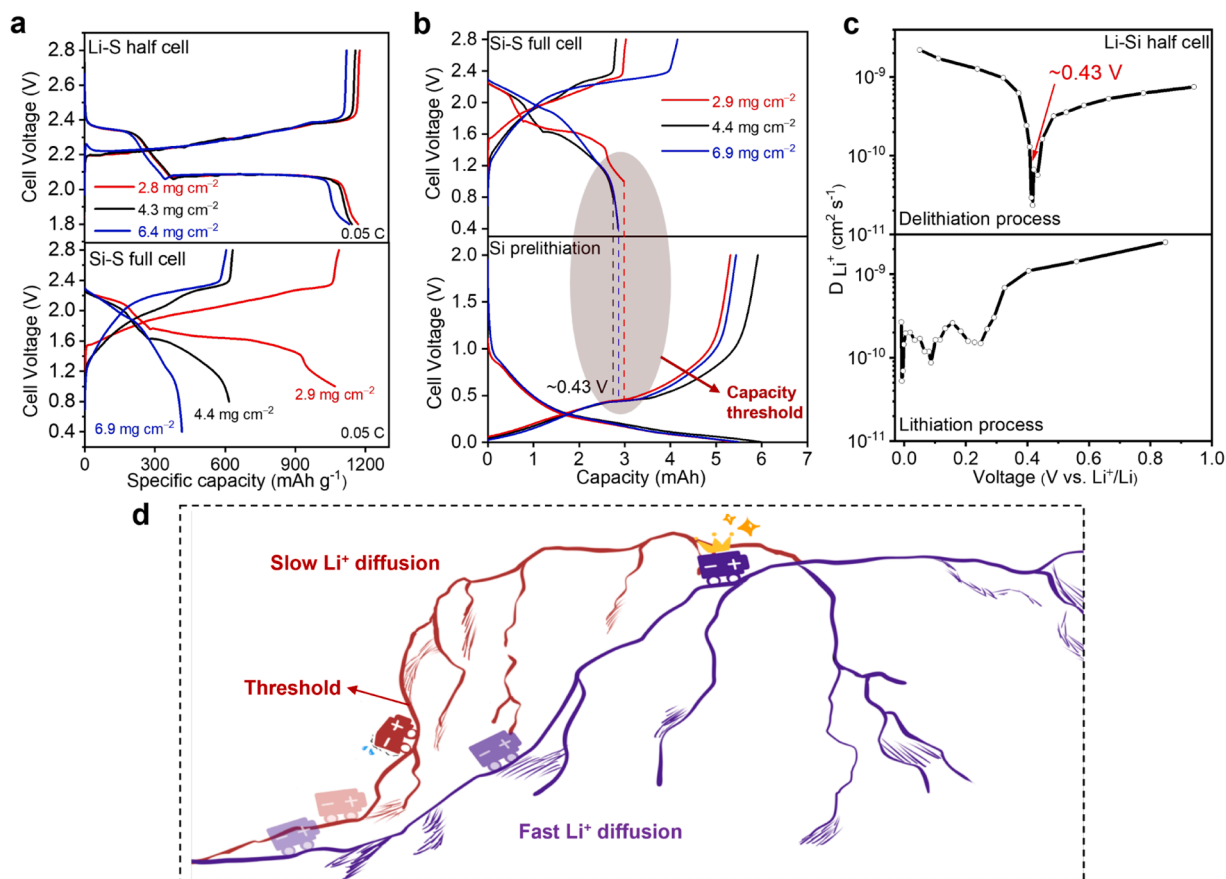


Fig. 1. Intrinsic origin of low capacity in Si-S battery. (a) Comparison of charge-discharge curves for Li-S half cells and Si-S full cells with varying S loadings, (b) Comparison of initial charge-discharge curves (top) for Si-S full cells at different S loadings and their corresponding prelithiation curves (bottom) for the silicon anodes, (c) Lithium diffusion coefficient of silicon anode as measured by GITT, plotted against voltage, (d) Schematic diagram of capacity threshold in Si-S full cells.

$$D = \frac{4}{\pi\tau} \left(\frac{m_B V_M}{M_B S} \right)^2 \left(\frac{\Delta E_S}{\Delta E_r} \right)^2$$

In this formulation, m_B denotes the active mass, M_B the molar mass, V_M the molar volume, and S the active surface area specific to silicon carbon electrodes. Additionally, τ , ΔE_S , ΔE_r , correspond to the pulse duration, the voltage shift between sequential steps and the voltage shift throughout the pulse interval. Notably, due to the simplification of the calculation process, the absolute values of Li⁺ diffusion coefficients may not be strictly precise. However, the comparison of their relative values remains meaningful [34]. The D profile with respect to voltage of the silicon anode in the charging (delithiation) process were established (Fig. 1c). It revealed that during the delithiation process of the silicon anode, the D reached a minimum value of approximately $2.36 \times 10^{-11} \text{ cm}^2 \text{ s}^{-1}$ at a voltage of around 0.43 V. The minimum value (Li_{1±0.25}Si) corresponds to the strong interaction between lithium and the host matrix during the delithiation process, potentially arising from the crystalline phase (c-LiSi) formed at high temperature [34–36]. However, since Li_{3.74}Si is the only crystalline phase that can form during silicon lithiation at room temperature, the phase correlated with reduced D is amorphous (a-LiSi). There is also a general trend that the D values in the voltage range between 0.01 V and 0.43 V are generally larger than those in the voltage range between 0.43 V and 1 V. These findings possibly suggest that the limiting factor for the full cell capacity is the extremely low D of the anode charged to around 0.43 V, as depicted in the schematic in Fig. 1d. As a result, increasing the sulfur loading and decreasing the NP ratio failed to exploit the potential capacity of the lithiated silicon anode when the voltage exceeded 0.43 V. We refer this unusual polarization effect at low current density as the “capacity threshold” in Si-S batteries.

2.2. Crossing the capacity threshold of Si-S battery via rapid Li⁺ diffusion

From the discussions above, it is evident that enhancing the lithium diffusion of the anodes could potentially increase the capacity release of the full cells. Here, we propose an intriguing protocol to achieve higher capacity release of Si-S full cells by fabricating a mud crack structured Si/C electrode with both high loading and rapid lithium-ion conduction behavior in a dry-slurry process method. In a typical procedure, the water-soluble binder, carboxymethylcellulose (CMC), is mixed with commercially-available Si/C anode material and a conductive agent, and then ball-milled thoroughly with the addition of water. Notably, the amount of water used is 16 ml mg⁻¹_{cmc}, much lower than that in conventional pre-dissolved CMC solutions (2 %, 49 ml mg⁻¹_{cmc}). The resulting “dry slurry” was then coated onto a 3D conductive carbon mesh substrate to make the Si/C anode, labeled as DS-Si (the morphology of the slurry is shown in Fig. 2a, inset). Due to the induced stress driven by solvent evaporation, some microcracks appeared on the electrode (Fig. 2a). The cross-sectional SEM image shows that these cracks can rupture through the electrode (Fig. 2b). In comparison, a conventional slurry preparation technique, in which 2 % pre-dissolved CMC was used as the binder with an additional excess of water, was employed to make the control Si/C anode with same loading as Fig. 2a, labeled as CS-Si (Fig. 2c). The Si anode used in the measurement in Fig. 1 was also made by the conventional method. The CT images further demonstrates the difference between DS-Si and CS-Si, revealing that the former has a through-thickness crack structure, while the latter lacks this feature (Fig. 2d). This structure can enhance the wettability of the electrolyte while maintaining the peeling strength of the electrode (Fig. 2e and f). Moreover, the graphite in silicon carbon materials contributes little to

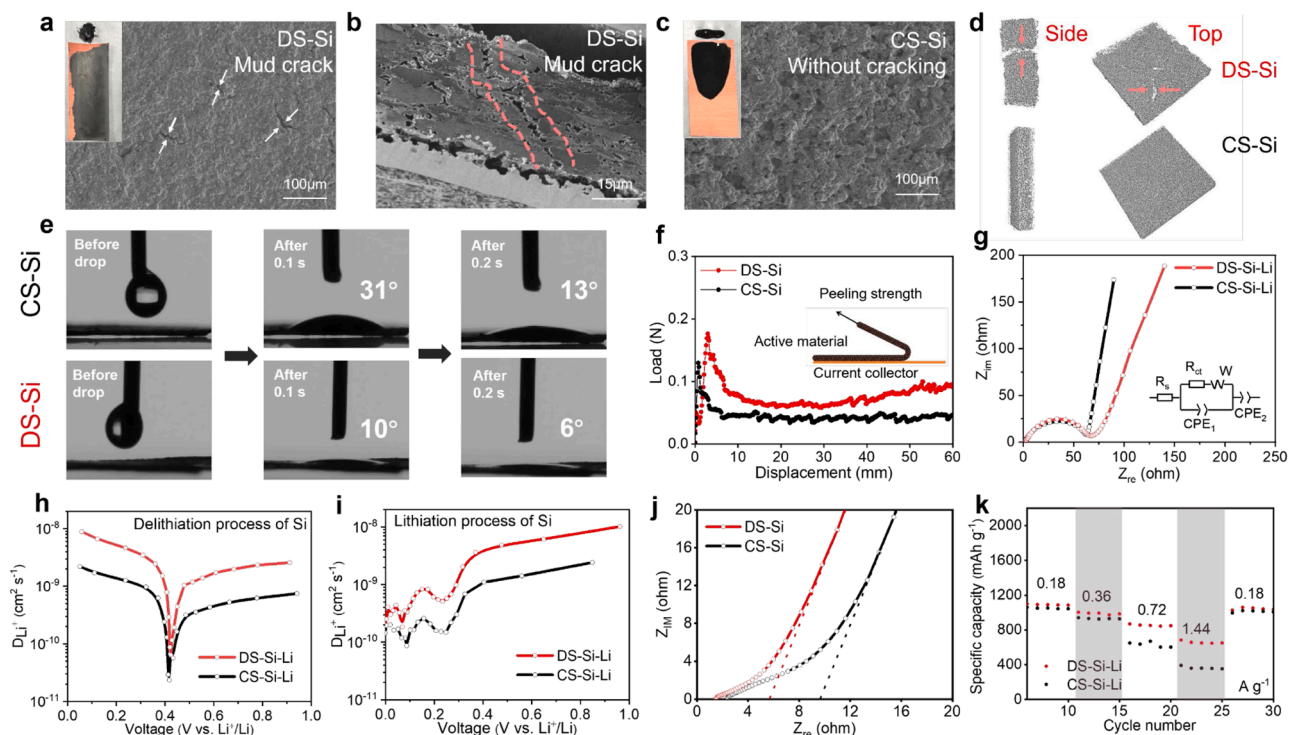


Fig. 2. Fast Li ion conduction in Si anode enables high-capacity Si-S battery. (a) Top-view SEM image of mud crack structured Si electrode fabricated by dry-slurry process, (b) Cross-sectional SEM image of mud crack structured Si electrode, (c) Top-view SEM image of Si electrode fabricated by conventional pre-dissolved process, (d) X-ray computed tomography image of Si electrode, (e) Testing of Contact angle of DS-Si and CS-Si, (f) Testing of peeling strength of DS-Si and CS-Si, (g) EIS curves for DS-Si and CS-Si, (h) A comparison of the lithium diffusion coefficients for DS-Si and CS-Si, as measured by GITT in charging process, (i) A comparison of the lithium diffusion coefficients for DS-Si and CS-Si, as measured by GITT in discharging process, (j) A comparison of the ion transport resistance tested by symmetric cells, (k) Comparison of the rate performance of DS-Si and CS-Si half cells.

the capacity in Li-S electrolyte but primarily serves to enhance conductivity and mitigate volume expansion (Fig. S2) [37]. We also examine the electrode structure after cycling and fully lithiated, as shown in Fig. S3. The DS-Si electrode shows densely packed particles with minimal empty space compared to CS-Si. Moreover, even at the fully lithiated state (maximum volume expansion), the anodes preserve the mud-crack structure. This indicates that, regardless of the lithiation stage, the anodes can sustain the structure and the cracks do not completely disappear despite the volume changes.

To further elucidate the advantages enabled by the DS-Si anode, the Li^+ diffusion coefficient of the Si/C anode made by different methods was examined via electrochemical impedance spectroscopy (EIS) and galvanostatic intermittent titration technique (GITT). The EIS curves of both anodes featured a semicircle in the high-frequency range followed by a linear segment in the low-frequency range. The simulation diagram contains R_s , R_{ct} , W , and CPE , representing the resistance of the electrolyte and electrode, the charge transfer resistance, the diffusion-controlled Warburg impedance and the double-layer capacitance, respectively [38]. Given that the silicon carbon material is consistent, the charge transfer resistances (R_{ct}) for both electrodes are nearly identical, measuring around 63 ohm (Fig. 2g). However, notable differences are observed in the lithium diffusion coefficients of the two types of electrodes. GITT was used to measure the D at various charging/discharging voltages of both anodes (the charge-discharge curves of the GITT are shown in Fig. S4). The D values of the DS-Si anode in both charging and discharging curves are larger than those of the CS-Si anode. Generally, the D values in the charging process showed smoother changes as the charging voltage varied. When the charging voltage reached approximately 0.43 V, both DS-Si and CS-Si anodes encountered a minimum D value (Fig. 2h). Notably, the DS-Si anode displayed a much larger D value ($6.7 \times 10^{-11} \text{ cm}^2 \text{ s}^{-1}$) at around 0.43 V, which is three times higher than that of the CS-Si ($2.3 \times 10^{-11} \text{ cm}^2 \text{ s}^{-1}$). During the

discharging process, the diffusion coefficient of DS-Si consistently exceeded that of CS-Si (Fig. 2i). As the voltage approaches 0 V, there is a significant fluctuation in the diffusion coefficient, which can be attributed to the formation of the crystalline phase of $\text{Li}_{15}\text{Si}_4$ [36]. Moreover, the ion transport resistance (R_{ion}) tested by symmetric cells shows a similar conclusion, with DS-Si electrode showing 12 ohm and CS-Si showing 18.6 ohm (Fig. 2j). Therefore, based on the data summarized in Tables S1 and S2, we calculated the tortuosity to be 6.3 for DS-Si and 9.1 for CS-Si. This suggests that the lithium-ion transport path in the DS-Si is shorter than in the CS-Si, which can be attributed to the straight cracks formed in the dry-processed electrode and its more compact structure. Thanks to the better Li^+ transport, the rate performance of the half-cell is also improved, showing higher capacity at various current densities (Fig. 2k).

2.3. Role of crossing the capacity threshold in enhancing Si-S battery performance

To verify the aforementioned hypothesis, the performance of the corresponding sulfur-based full cells were measured. First, prelithiation curves of both Si/C electrode half cells were conducted, and the results revealed that the charging and discharging (delithiation and lithiation) capacities showed negligible difference, with differences of 0.32 mAh and 0.41 mAh, respectively. This indicated that the overall lithium content in the Si/C anodes, which served as the lithium source in Si-S full cells, was the same. When matched with the conventional sulfur cathodes with a sulfur loading of approximately 4.3 mg cm^{-2} and a 1.2 NP ratio, the corresponding Si-S full cells showed dramatically different capacities (Fig. 3a). Full cell with CS-Si can only deliver a capacity of 3.2 mAh (763 mAh g^{-1}), which is 53 % of the prelithiation capacity. In contrast, the full cell prepared with DS-Si can release about 5.0 mAh (1148 mAh g^{-1}), accounting for 78 % of the prelithiation capacity. The

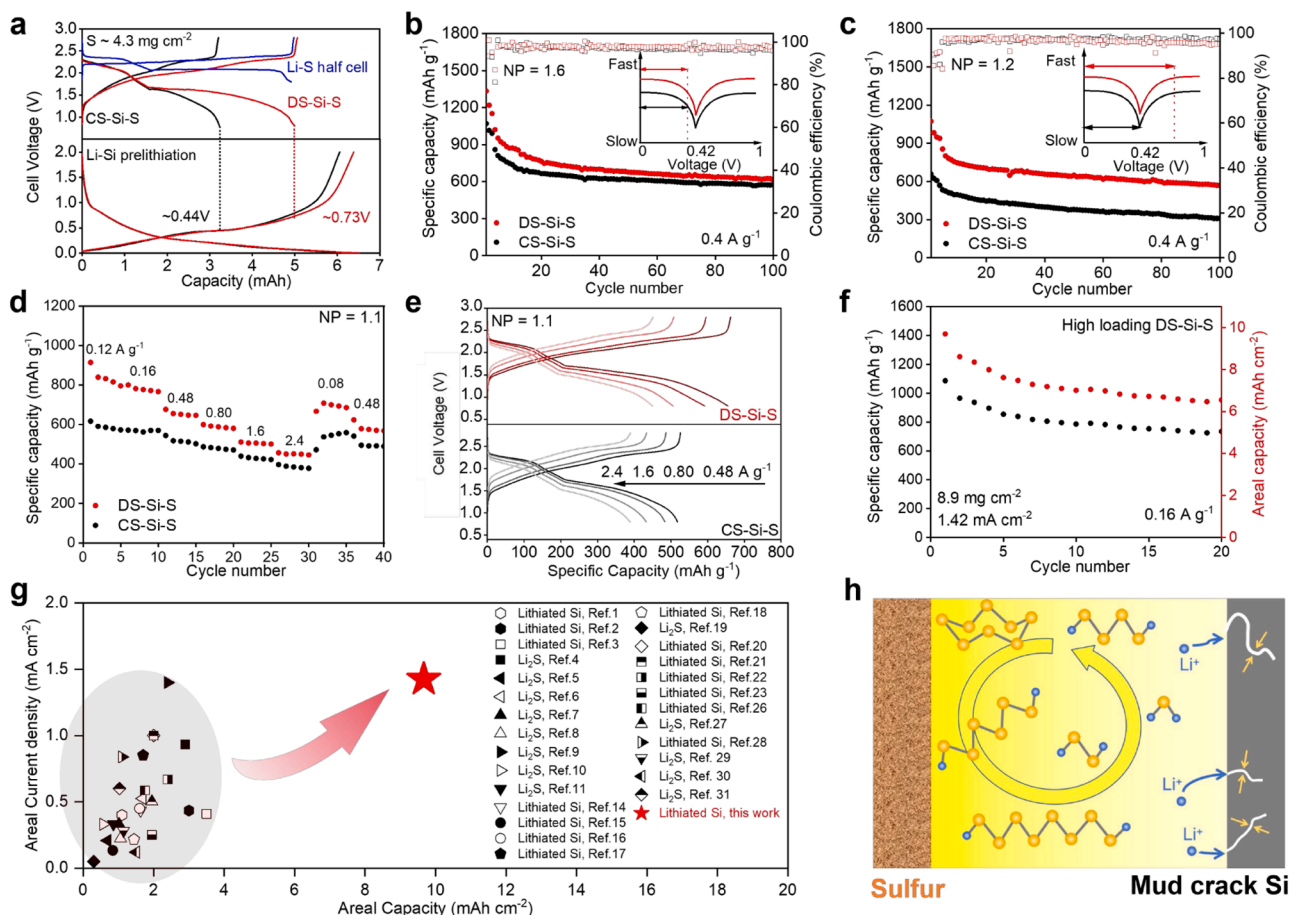


Fig. 3. Electrochemical performance of high-capacity Si-S coin cells. (a) Comparison of the charge-discharge curves of DS-Si-S and CS-Si-S full cells with the corresponding prelithiation curves, (b) Comparison of the cycling performance of different Si-S full cells under a 1.6 NP ratio, (c) Comparison of the cycling performance of different Si-S full cells under a 1.2 NP ratio, (d) Comparison of the rate performance of different Si-S full cells under a 1.1 NP ratio, (e) Charge-discharge curves of DS-Si-S and CS-Si-S under various current density, (f) Cycling performance of high loading DS-Si-S, (g) Comparison diagram with previous work in Si-S batteries (the references are provided in Table S3), (h) Schematic diagram of the full cell with S cathode and mud crack Si anode.

charging voltage of the Si/C anode in the DS-Si based full cell could surpass the threshold of the CS-Si (0.43 V) to reach 0.73 V, indicating the excellent lithium utilization efficiency of the full cell prepared with DS-Si. As discussed in Fig. 1, the minimum D value at the charging voltage of 0.43 V accounts for the capacity threshold of the Si-S battery. Due to the much larger D values of the DS-Si at 0.43 V, the more rapid Li^+ conduction in the DS-Si enables the corresponding Si-S full battery to surpass the capacity threshold, consequently realizing better utilization of the cathode materials and a much higher capacity release. This can also be identified by the capacity comparison between the S||Li and S||DS-Si with the same sulfur loading, where the capacity of S||DS-Si is almost the same as that of the S||Li half cell (Fig. 3a). This result suggests that a similar sulfur utilization ratio can be achieved, whether using a DS-Si or a Li metal anode.

To verify the important role of crossing such capacity threshold in the overall performance, Si-S coin cells with different sulfur loadings and NP ratios were assembled and evaluated. All the cells employed the same sulfur cathode, in which Titanium boride (TiB_2) powders were applied as a catalyst to mitigate the polysulfide shuttling effects and facilitate the conversion of soluble Li_2S_4 into insoluble Li_2S (Fig. S5) [39], and the Si/C anodes made by the dry-slurry and conventional-slurry processes were used for comparison (the Li-Si half cells are shown in Fig. S6). When the sulfur loading is relatively low (for example 2.9 mg cm^{-2}) and the NP ratio is high (for example $\text{NP} = 1.6$), the Si-S cells based on different Si/C anodes showed small difference in terms of the capacity and cycling performance. The initial capacity of

DS-Si-S is 1334 mAh g^{-1} , slightly higher than the 1070 mAh g^{-1} of CS-Si-S (Fig. S7a). After 100 cycles, the specific capacities of both cells tend to converge, reaching 610 mAh g^{-1} and 572 mAh g^{-1} , respectively (Fig. 3b). In contrast, as the NP ratio decreases and the sulfur loading increases, a significant difference in the specific capacity of the full cells was presented (Figs. S7b and 3c). When the NP ratio increased to 1.2 and mass loading of sulfur increased to 4.2 mg cm^{-2} , the DS-Si based Si-S full cell exhibited a large initial capacity of 1073 mAh g^{-1} , which far exceeded the capacity of the CS-Si based full cell (658 mAh g^{-1}), as shown in Fig. 3c. During subsequent cycles, the specific capacity of DS-Si based full cell remained significantly higher than that of CS-Si based full cell. After 100 cycles, the specific capacities of the full cells are 568 mAh g^{-1} and 309 mAh g^{-1} , respectively. To examine the origin for such dramatic differences in the initial specific capacity and the specific capacity after 100 cycles, the delithiation states of both Si anodes in the corresponding full cells were measured. With an NP ratio of 1.6, the initial capacities of DS-Si-S and CS-Si-S are 3.19 and 2.67 mAh, corresponding to the delithiation voltage of Si anodes around 0.43 V (Fig. S8a). The long plateaus in the discharge curves of the full cells indicate the complete conversion of polysulfides to Li_2S . This means that when the NP ratio is high and the sulfur loading is low, the limited sulfur loading restricts the capacity of the full cell. In other words, the lithium content in the lithiated silicon within the 0–0.43 V range is sufficient to support the cathode capacity without the necessity to surpass the capacity threshold of the silicon anode (Fig. 3b inset). And the small difference in specific capacities is probably due to the difference in diffusion coefficients of the silicon

anodes within the 0–0.43 V range. However, with an NP ratio of 1.2, the initial capacities of DS-Si-S and CS-Si-S are 4.48 mAh and 2.76 mAh, corresponding to the delithiation voltages of 0.80 V and 0.43 V of the silicon anodes, respectively (Fig. S8 b). It is clear that DS-Si-S can surpass the capacity threshold, while CS-Si-S cannot. This indicates that sulfur loading is not the limiting factor for the full cell capacity under low NP ratio and high sulfur loading. Instead, the ability to surpass the capacity threshold results in the significant capacity difference (Fig. 3c inset). The substantial difference in specific capacity at lower NP ratio and higher sulfur loading further underscores the importance of surpassing the capacity threshold in Si-S batteries.

Thanks to the mud crack structural feature and the enhanced Li^+ diffusion coefficient in the DS-Si anode, the DS-Si based full cell exhibited better rate capability. As shown in Fig. 3d and e, the specific capacities of DS-Si-S consistently surpass those of CS-Si-S under various current densities. This pattern is mirrored in the half cells, where the specific capacities of DS-Si-Li remain higher than those of CS-Si-Li at all tested current densities. Moreover, based on this dry-slurry preparation method, we attempted to push the sulfur loading to its limits. To ensure an adequate lithium source, high-loading prelithiated anode was prepared by the dry-slurry process. As a result, the Si-S battery can achieve 9.7 mAh cm^{-2} at 8.9 mg cm^{-2} (Fig. 3f). For comparison, we have reviewed previous work and listed in Table S3. Lithium sources for Si-S batteries are divided into two types: lithiated silicon and Li_2S . Currently,

most work only presents Si-S batteries as supplementary data for the delicate design of S cathodes and Si anodes to demonstrate their feasibility, lacking systematic research. It is noteworthy that for practical application, specific capacity, average voltage, and sulfur loading must meet certain standards. Sacrificing one factor to improve another cannot meet the requirements for achieving high energy density. Our work achieves a discharge specific capacity of 1086 mAh g^{-1} with a sulfur loading of 8.9 mg cm^{-2} and a voltage range of 0.8–2.8V. From the current density and areal capacity perspectives, our work achieved much improved performance than most of the previous works (Fig. 3g). Therefore, for Si-S battery with high loading and low NP ratio, achieving capacity release requires not only an adequate lithium source but also a better electrode structural design to ensure efficient anode charge transport properties (Fig. 3h).

2.4. Advantages of Si-S battery at practical level

Next, pouch cell tests were conducted to verify the practicality of Si-S batteries (Fig. 4a). To further understand the impact of electrolyte conditions on performance, different electrolyte-to-sulfur (E/S) ratio of $5 \mu\text{L mg}^{-1}$ and $15 \mu\text{L mg}^{-1}$ were employed in the testing of Si-S pouch cell, as illustrated in Fig. 4b. The breakpoints in the black line are due to a power outage. These ratios specifically represent lean and excess electrolyte conditions, respectively. When the E/S ratio is set at 15, the

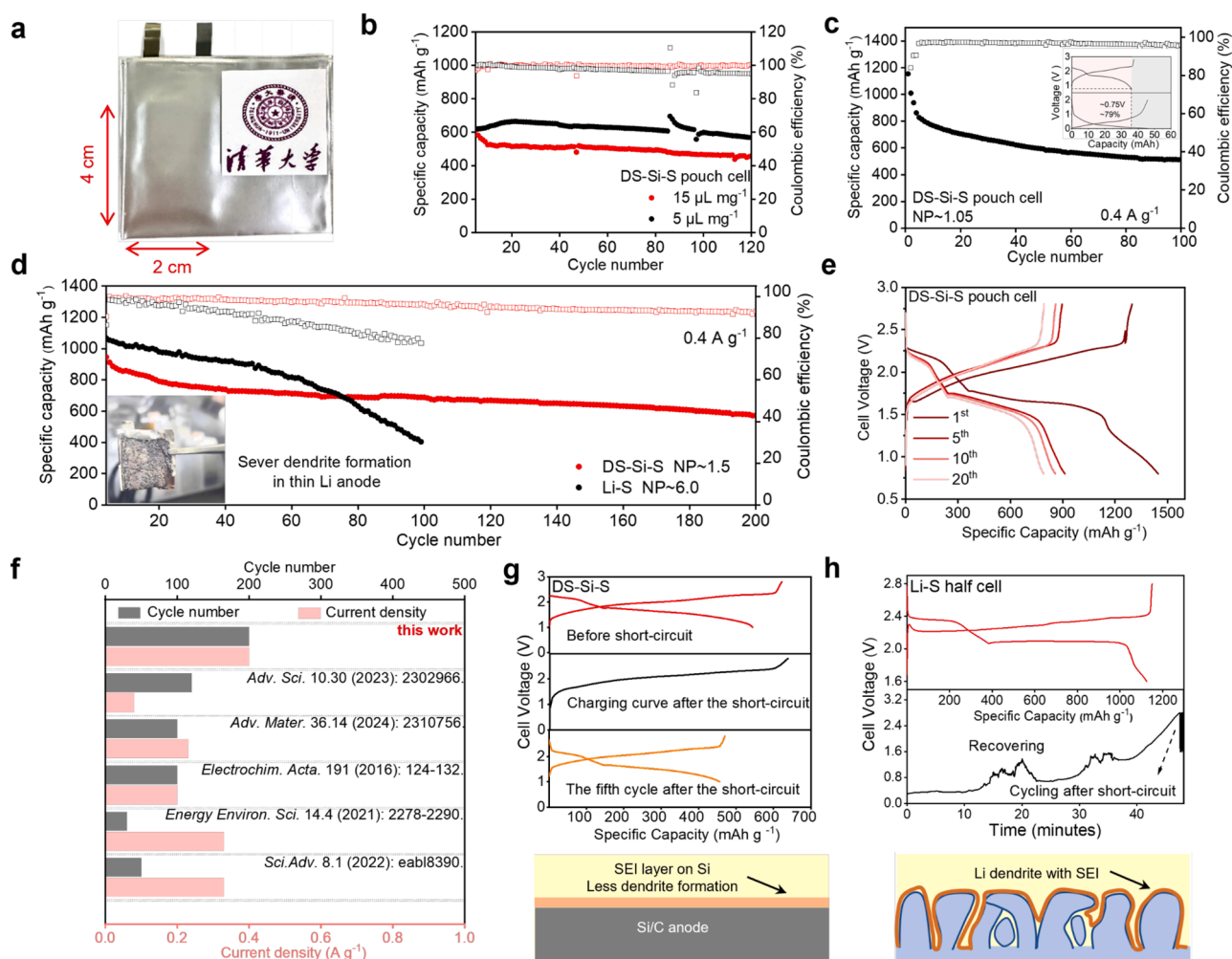


Fig. 4. Electrochemical performance of high-capacity Si-S pouch cells. (a) Image of Si-S pouch cell, (b) Comparative cycling performance of Si-S pouch cells with varying E/S ratio, (c) Cycling performance of Si-S pouch cell under a 1.05 NP ratio, (d) Comparison of the cycling performance of Si-S and Li-S pouch cells under a 3.0 mg cm^{-2} sulfur loading, (e) Charge-discharge curves for Si-S pouch cell, (f) Performance comparison of previous Si-S pouch cells, (g) External short-circuit test of Si-S full cell, (h) External short-circuit test of Li-S half cell.

initial discharge curve of Si-S full cell exhibits two distinct plateaus (Fig. S9a). The upper plateau corresponds to the reduction of elemental sulfur into soluble long-chain polysulfides, such as Li_2S_8 and Li_2S_6 . Following this, the lower plateau corresponds to the further reduction of these soluble polysulfides, which leads to the formation of solid reduction products on the carbon matrix (Li_2S). In contrast, when the E/S ratio is reduced to 5, the specific capacity of the upper plateau significantly decreases to 207 mAh g^{-1} . And the lower plateau demonstrates considerable polarization. Additionally, a lean electrolyte demonstrates higher stable specific capacity of 660 mAh g^{-1} and requires longer activation process. Conversely, an excess of electrolyte leads to increased dissolution of polysulfides, resulting in lower stable specific capacity of 520 mAh g^{-1} . Despite this, the excess electrolyte condition manages to maintain greater stability during prolonged cycling (Fig. S9b). This suggests a trade-off between early performance and long-term stability based on electrolyte volume. Subsequently, we assembled pouch cells with moderate amount of electrolyte ($10 \mu\text{L mg}^{-1}$). By reducing the NP ratio to 1.05 and increasing the sulfur loading, we achieved outcomes comparable to those observed in coin cells. DS-Si-S pouch cell was able to surpass the capacity threshold, effectively utilizing 79 % of the prelithiation capacity, and demonstrated stable performance in subsequent cycles (Fig. 4c).

At the practical level, the superiority of Si-S batteries can be further highlighted. In lithium sulfur coin cell, significant excess lithium and extremely high NP ratios (>150) are often employed to achieve higher stability and specific capacity. For instance, the lithium foil is typically thicker than $500 \mu\text{m}$ in coin cell testing, ensuring that the anode does not affect the overall performance. However, in practical lithium sulfur pouch cells, lower NP ratios and thin lithium anodes are necessary to reach higher energy density. This thin lithium anode often leads to poor cycle stability and safety risks. Under an NP ratio of 6 ($90 \mu\text{m}$ lithium foil), the capacity and coulombic efficiency of Li-S pouch cell decline rapidly after 60 cycles, which can be attributed to the pulverization and failure of the thin lithium anode (Figs. 4d and S10) [40,41]. On the contrary, Si-S pouch cell exhibits better cycling stability under the same sulfur loading and current density. To ensure the same anode loading as Li-S pouch cell, the NP ratio of Si-S pouch cell is set to 1.5 (calculated based on the mass of the fully lithiated Si/C anode). Si-S pouch cell achieves a specific capacity of 912 mAh g^{-1} at 400 mA g^{-1} , maintaining 690 mAh g^{-1} without experiencing rapid decay after 200 cycles (Fig. 4d and e). The result exceeds most of the previous Si-S and Graphite-S pouch cells (Fig. 4f). The energy density based on cathode and anode material can reach 537 Wh kg^{-1} . Apart from that, we evaluated the safety performance of Si-S batteries in coin cells. By directly connecting the cathode and anode with a copper wire for two hours before charging, we found that the Si-S battery could still recover and cycle effectively (Fig. 4g). Conversely, as shown in Fig. 4h, Li-S battery failed to recover after similar short-circuit testing, highlighting the remarkable resilience of Si-S batteries. The high stability and energy density of Si-S pouch cell highlights the potential for practical applications.

3. Conclusions

In this work, we explored the factors that restrict the capacity release of Si-S batteries. We found that the major limitation under conditions of high sulfur loading and low NP ratios is the slow lithium diffusion capability of the silicon anode. Also, we uncovered a phenomenon known as the capacity threshold, where no matter how much the sulfur loading is increased, the full cell capacity is only able to release a capacity fixed by the lithiated silicon anode. To overcome this limitation, we developed a dry-slurry process for preparing silicon electrode with mud-crack structure and successfully fabricated Si-S batteries that break through this capacity threshold. This approach not only significantly increases the sulfur loading but also reduces the NP ratio without sacrificing the electrochemical performance. The resulting Si-S full cell could reach a high areal capacity of 9.7 mAh cm^{-2} at 8.9 mg cm^{-2} .

Moreover, the Si-S pouch cell demonstrated improved cycling performance compared to Li-S pouch cell, maintaining a specific capacity of $\sim 600 \text{ mAh g}^{-1}$ after 200 cycles. Consequently, this work reveals that the charge transfer of silicon anodes plays a critical role in the capacity release of Si-S full cells, providing new insights for the design principle of Si-S batteries.

4. Methods

Cathode preparation: Sulfur carbon composites were synthesized with a conventional melting-infusion process. After the uniform mixing of ordered mesoporous carbon (CMK-3) and sulfur powder, the mixture was heated to $155 \text{ }^\circ\text{C}$ and maintained for 12 h. The mass ratio of CMK-3 to sulfur was 7:3. To get the cathode slurry, sulfur carbon composite, TiB_2 , CNT and polyvinylidene fluoride binder (PVDF) were well-mixed with a mass ratio of 72:8:10:10 in N-methyl-2-pyrrolidone (NMP) solvent. Carbon felts were cut into circular pieces with a diameter of 12 mm and served as the current collector, onto which the slurry was cast and left to dry overnight at $70 \text{ }^\circ\text{C}$.

Anode preparation: For dry-process slurry: Silicon carbon powders (purchased from Btr New Material Group Co.,Ltd.), carbon black and Carboxymethylcellulose powder (CMC) were uniformly mixed in a mass ratio of 8:1:1. Subsequently, $16.7 \text{ ml mg}_{\text{cmc}}^{-1}$ water was added, and the mixture underwent ball milling to achieve a homogeneous dry slurry. For the conventional slurry, after mixing the silicon carbon and carbon black powders, 2 % pre-dissolved CMC and excess water were added. The mixture was stirred to achieve a uniform slurry with a consistent mass ratio. After each preparation, we take samples from different areas, weigh them before and after drying, and check if the weight ratios are consistent. If they are, it confirms that the slurry is well-mixed. Similarly, the slurry was cast onto carbon felts (the same size as the cathode) and dried at $105 \text{ }^\circ\text{C}$ overnight to obtain anodes.

Assembly of Si-S coin cells: Firstly, Si/C anodes were prelithiated in half cells, using lithium metal as the counter electrode. Si/C half cells were cycled between 5 mV and 2 V four times at 90 mA g^{-1} and discharged to 5 mV. The electrolyte was 1 M lithium bis(trifluoromethanesulfonyl)imide (LiTFSI) in 1,3-dioxolane/1,2-dimethoxyethane (1:1, v/v) with 0.2 M LiNO_3 . During the prelithiation process, an excess amount of electrolyte was employed. After that, the as-obtained lithiated Si/C anode was assembled with a sulfur cathode into a CR2032 coin cell in an Ar-filled glove box. An additional of electrolyte were introduced into the sulfur cathode. The full cells were cycled between 1.0 and 2.8 V. Under high loading conditions, the cycling range was adjusted to 0.8–2.8 V. Notably, to mitigate the influence of current magnitude, the activation currents in the full cells were maintained below those in the prelithiation process. Based on the specific capacity of the half cells shown in Fig. S7, we assume a sulfur cathode utilization rate of 72 %. The NP ratio is defined as the mass of the sulfur cathode multiplied by 1200 mAh g^{-1} and divided by the prelithiation capacity of the silicon anode. In other words, once the prelithiation capacity and the NP ratio are determined, the sulfur loading can be calculated. Additionally, during the battery test, $1\text{C}=1675 \text{ mA g}^{-1}$.

Assembly of S-Li coin cells: S@C@ TiB_2 cathodes were assembled in coin cells, with Li foils as counter electrodes. The voltage window of S-Li half cells was 1.6–2.8 V.

Assembly of Si-Li coin cells: Silicon carbon anodes were assembled in coin cells, with Li foils as counter electrodes. The cycling voltage window of Si-Li coin cells was 0.005–2 V.

Assembly of S-Si pouch cell: First, carbon felts were cut into $2 \times 4 \text{ cm}^2$ and $1.9 \times 3.9 \text{ cm}^2$ sizes. The anode and cathode slurries were uniformly coated onto the substrate, and then dried to obtain the cathode and anode sheets. After that, lithium foils measuring $2.1 \times 4.1 \text{ cm}^2$ were used as counter electrodes, and half cells were assembled for prelithiation. The prelithiation current density and cycling number were consistent with those in coin cells. Subsequently, a certain amount of

electrolyte was added to the cathode, and the prelithiated anode was assembled with the sulfur cathode to form a full cell, which was then sealed in aluminum-plastic film. The voltage window of S-Si pouch cells was 0.8–2.8 V.

Galvanostatic Intermittent Titration Technique (GITT) Analysis: GITT was employed to evaluate the lithium diffusivity of Si-Li half cells. With a consistent load, the batteries were subjected to current pulse intervals at 90 mA g⁻¹ for 0.5 h, followed by 2.5 h resting periods, until complete discharge or charge. The voltage window ranged from 5 mV to 2 V. In GITT test, copper foils were used as the current collector.

Short-Circuit Test: S-Si full cell and S-Li half cells underwent a 3-hour short-circuit using copper wire. Following this, recovery charging was conducted at a current density of 480 mA g⁻¹, followed by subsequent cycling.

Material Characterization: The morphology of silicon carbon electrodes was observed by a HITACHI SU8010 field emission scanning electron microscope (SEM). Thermogravimetric analysis (TGA) was conducted in the air with a TGA-1000B, Shanghai Innuo Precision Instruments Co., Ltd. The temperature ranges from 25 to 1000 °C, with a heating rate of 10 °C min⁻¹. Upon reaching 1000 °C, the temperature was maintained for 50 min to ensure complete removal of carbon.

Energy density calculation for Si-S battery: Assuming a sulfur utilization rate of 75 % and a silicon utilization rate of 35 %, with sulfur comprising 70 % of the cathode mass and silicon comprising 70 % of the anode mass. Additionally, the full cell's E/S ratio is 3, the N/P ratio is 1.1, and the average discharge voltage is 1.8 V, with the mass of the current collector and separator remaining unchanged. It should be noted that this is a simplified energy density calculation, which means that the exact values may vary, but the trend of energy density changing with sulfur mass remains consistent.

S loading	Electrolyte	Cathode	Silicon	Anode	Current collector + Separator	Energy density (Wh kg ⁻¹)
1.0	3.0	1.4	0.9	1.3	3.4	247.2
2.0	6.0	2.9	1.8	2.6	3.4	303.7
3.0	9.0	4.3	2.8	3.9	3.4	328.7
4.0	12.0	5.7	3.7	5.3	3.4	342.8
5.0	15.0	7.1	4.6	6.6	3.4	351.9
6.0	18.0	8.6	5.5	7.9	3.4	358.2
7.0	21.0	10.0	6.4	9.2	3.4	362.9
8.0	24.0	11.4	7.4	10.5	3.4	366.5
9.0	27.0	12.9	8.3	11.8	3.4	369.3
10.0	30.0	14.3	9.2	13.2	3.4	371.6

Unit: mg cm⁻² (except for energy density)

CRedit authorship contribution statement

Zhaotian Xie: Writing – original draft, Methodology, Investigation, Formal analysis, Data curation, Conceptualization. **Wentao Zhang:** Writing – review & editing, Investigation, Formal analysis, Data curation, Conceptualization. **Xin He:** Writing – review & editing, Investigation, Data curation, Conceptualization. **Ziyao Gao:** Investigation, Data curation, Conceptualization. **Zhicheng Du:** Writing – review & editing, Investigation. **Hongkai Yang:** Investigation, Data curation. **Xinming Zhang:** Investigation. **Rui li:** Writing – review & editing, Data curation. **Yanbing He:** Writing – review & editing, Resources. **Lele Peng:** Writing – review & editing, Supervision, Resources, Investigation, Funding acquisition. **Feiyu Kang:** Writing – review & editing, Supervision, Resources, Project administration, Funding acquisition, Conceptualization.

Declaration of competing interest

The authors declare that they have no known competing financial interests or personal relationships that could have appeared to influence

the work reported in this paper.

Acknowledgments

This work was financially supported by Scientific Research Start-up Funds of Tsinghua SIGS (Grant No. QD2021018C to L.P.), the National Natural Science Foundation of China (Grant No. 20231710015 and No. 22209096 to L.P.), Guangdong Basic and Applied Basic Research Foundation (Grant No. 2023A1515010059 to L.P.), Shenzhen Outstanding Talents Training Fund and Shenzhen Fundamental Research Program (Grant No. JCYJ20220530143003008 to F.K.). The authors also acknowledge the Materials and Devices Testing Center at Tsinghua Shenzhen International Graduate School, Shenzhen 518055, China.

Supplementary materials

Supplementary material associated with this article can be found, in the online version, at [doi:10.1016/j.enstm.2025.104046](https://doi.org/10.1016/j.enstm.2025.104046).

Data availability

The data that support the findings of this study were available from the corresponding author upon reasonable request.

References

- [1] D. Larcher, J.M. Tarascon, Towards greener and more sustainable batteries for electrical energy storage, *Nat. Chem.* 7 (2015) 19–29, <https://doi.org/10.1038/nchem.2085>.
- [2] J.B. Goodenough, K.S. Park, The Li-Ion rechargeable battery: a perspective, *J. Am. Chem. Soc.* 135 (2013) 1167–1176, <https://doi.org/10.1021/ja3091438>.
- [3] V. Etacheri, R. Marom, R. Elazari, G. Salitra, D. Aurbach, Challenges in the development of advanced Li-ion batteries: a review, *Energy Environ. Sci.* 4 (2011) 3243–3262, <https://doi.org/10.1039/C1EE01598B>.
- [4] P.G. Bruce, S.A. Freunberger, L.J. Hardwick, J.M. Tarascon, Li–O₂ and Li–S batteries with high energy storage, *Nat. Mater.* 11 (2012) 19–29, <https://doi.org/10.1038/nmat3191>.
- [5] M. Wang, Z. Bai, T. Yang, C. Nie, X. Xu, Y. Wang, J. Yang, S. Dou, N. Wang, Advances in high sulfur loading cathodes for practical lithium-sulfur batteries, *Adv. Energy Mater.* 12 (2022) 2201585, <https://doi.org/10.1002/aenm.202201585>.
- [6] Y. Yang, M.T. McDowell, A. Jackson, J.J. Cha, S.S. Hong, Y. Cui, New nanostructured Li₂S/silicon rechargeable battery with high specific energy, *Nano Lett.* 10 (2010) 1486–1491, <https://doi.org/10.1021/nl100504q>.
- [7] Y. Chen, T. Wang, H. Tian, D. Su, Q. Zhang, G. Wang, Advances in lithium–sulfur batteries: from academic research to commercial viability, *Adv. Mater.* 33 (2021) 2003666, <https://doi.org/10.1002/adma.202003666>.
- [8] P. Shi, X.Q. Zhang, X. Shen, R. Zhang, H. Liu, Q. Zhang, A review of composite lithium metal anode for practical applications, *Adv. Mater. Technol.* 5 (2020) 1900806, <https://doi.org/10.1002/admt.201900806>.
- [9] G. Zhou, H. Chen, Y. Cui, Formulating energy density for designing practical lithium–sulfur batteries, *Nat. Energy* 7 (2022) 312–319, <https://doi.org/10.1038/s41560-022-01001-0>.
- [10] X.B. Cheng, R. Zhang, C.Z. Zhao, Q. Zhang, Toward safe lithium metal anode in rechargeable batteries: a review, *Chem. Rev.* 117 (2017) 10403–10473, <https://doi.org/10.1021/acs.chemrev.7b00115>.
- [11] R. Chen, T. Zhao, F. Wu, From a historic review to horizons beyond: lithium–sulfur batteries run on the wheels, *Chem. Commun.* 51 (2015) 18–33, <https://doi.org/10.1039/C4CC05109B>.
- [12] L. Chen, L.L. Shaw, Recent advances in lithium–sulfur batteries, *J. Power Sources* 267 (2014) 770–783, <https://doi.org/10.1016/j.jpowsour.2014.05.111>.
- [13] L. Peng, Z. Wei, C. Wan, J. Li, Z. Chen, D. Zhu, D. Baumann, H. Liu, C.S. Allen, X. Xu, A.I. Kirkland, I. Shakir, Z. Almutairi, S. Tolbert, B. Dunn, Y. Huang, P. Sautet, X. Duan, A fundamental look at electrocatalytic sulfur reduction reaction, *Nat. Catal.* 3 (2020) 762–770, <https://doi.org/10.1038/s41929-020-0498-x>.
- [14] A. Manthiram, Y. Fu, S.H. Chung, C. Zu, Y.S. Su, Rechargeable lithium–sulfur batteries, *Chem. Rev.* 114 (2014) 11751–11787, <https://doi.org/10.1021/cr500062v>.
- [15] Q. Pang, X. Liang, C.Y. Kwok, L.F. Nazar, Advances in lithium–sulfur batteries based on multifunctional cathodes and electrolytes, *Nat. Energy* 1 (2016) 16132, <https://doi.org/10.1038/nenergy.2016.132>.
- [16] M. Zhao, B.Q. Li, X.Q. Zhang, J.Q. Huang, Q. Zhang, A perspective toward practical lithium–sulfur batteries, *ACS Cent. Sci.* 6 (2020) 1095–1104, <https://doi.org/10.1021/acscentsci.0c00449>.

- [17] S. Nanda, A. Manthiram, Lithium degradation in lithium–sulfur batteries: insights into inventory depletion and interphasial evolution with cycling, *Energy Environ. Sci.* 13 (2020) 2501–2514, <https://doi.org/10.1039/D0EE01074J>.
- [18] C.X. Bi, L.P. Hou, Z. Li, M. Zhao, X.Q. Zhang, B.Q. Li, Q. Zhang, J.Q. Huang, Protecting lithium metal anodes in lithium–sulfur batteries: a review, *Energy Mater. Adv.* 4 (2023) 0010, <https://doi.org/10.34133/energymatadv.0010>.
- [19] H. Hong, N.A.R. Che Mohamad, K. Chae, F.M. Mota, D.H. Kim, The lithium metal anode in Li–S batteries: challenges and recent progress, *J. Mater. Chem. A* 9 (2021) 10012–10038, <https://doi.org/10.1039/D1TA01091C>.
- [20] X. Liang, J. Yun, Y. Wang, H. Xiang, Y. Sun, Y. Feng, Y. Yu, A new high-capacity and safe energy storage system: lithium-ion sulfur batteries, *Nanoscale* 11 (2019) 19140–19157, <https://doi.org/10.1039/C9NR05670J>.
- [21] K. Eom, J.T. Lee, M. Oschatz, F. Wu, S. Kaskel, G. Yushin, T.F. Fuller, A stable lithiated silicon–chalcogen battery via synergetic chemical coupling between silicon and selenium, *Nat. Commun.* 8 (2017) 13888, <https://doi.org/10.1038/ncomms13888>.
- [22] M.T. McDowell, S.W. Lee, W.D. Nix, Y. Cui, 25th Anniversary article: understanding the lithiation of silicon and other alloying anodes for lithium-ion batteries, *Adv. Mater.* 25 (2013) 4966–4985, <https://doi.org/10.1002/adma.201301795>.
- [23] X. Zhang, Y. Yang, Z. Zhou, Towards practical lithium-metal anodes, *Chem. Soc. Rev.* 49 (2020) 3040–3071, <https://doi.org/10.1039/C9CS00838A>.
- [24] J. Lee, G. Oh, H.Y. Jung, J.Y. Hwang, Silicon anode: a perspective on fast charging lithium-ion battery, *Inorganics* 11 (2023) 182, <https://doi.org/10.3390/inorganics11050182> (Basel).
- [25] M. Alidoost, A. Mangini, F. Caldera, A. Anceschi, J. Amici, D. Versaci, L. Fagiolarì, F. Trotta, C. Francia, F. Bella, S. Bodoardo, Micro-Mesoporous carbons from cyclodextrin nanosponges enabling high-capacity silicon anodes and sulfur cathodes for lithiated Si–S batteries, *Chem. Eur. J.* 28 (2022) e202104201, <https://doi.org/10.1002/chem.202104201>.
- [26] R. Mo, Z. Lei, D. Rooney, K. Sun, Anchored monodispersed silicon and sulfur nanoparticles on graphene for high-performance lithiated silicon–sulfur battery, *Energy Storage Mater.* 23 (2019) 284–291, <https://doi.org/10.1016/j.ensm.2019.04.046>.
- [27] J. Brückner, S. Thieme, F. Böttger-Hiller, I. Bauer, H.T. Grossmann, P. Strubel, H. Althues, S. Spange, S. Kaskel, Carbon-based anodes for lithium sulfur full cells with high cycle stability, *Adv. Funct. Mater.* 24 (2014) 1284–1289, <https://doi.org/10.1002/adfm.201302169>.
- [28] A. Krause, S. Dörfler, M. Piwko, F.M. Wisser, T. Jaumann, E. Ahrens, L. Giebeler, H. Althues, S. Schädlich, J. Grothe, A. Jeffery, M. Grube, J. Brückner, J. Martin, J. Eckert, S. Kaskel, T. Mikolajick, W.M. Weber, High area capacity lithium–sulfur full-cell battery with prelithiated silicon nanowire–carbon anodes for long cycling stability, *Sci. Rep.* 6 (2016) 27982, <https://doi.org/10.1038/srep27982>.
- [29] J. Zhao, G. Zhou, K. Yan, J. Xie, Y. Li, L. Liao, Y. Jin, K. Liu, P.C. Hsu, J. Wang, H. M. Cheng, Y. Cui, Air-stable and freestanding lithium alloy/graphene foil as an alternative to lithium metal anodes, *Nat. Nanotechnol.* 12 (2017) 993–999, <https://doi.org/10.1038/nnano.2017.129>.
- [30] L. Zhang, C. Zhao, Q. Jian, M. Wu, T. Zhao, A high-performance lithiated silicon–sulfur battery with pomegranate-structured electrodes, *J. Power Sources* 506 (2021) 230174, <https://doi.org/10.1016/j.jpowsour.2021.230174>.
- [31] U. Zubair, J. Amici, S.M. Crespiara, C. Francia, S. Bodoardo, Rational design of porous carbon matrices to enable efficient lithiated silicon sulfur full cell, *Carbon* 145 (2019) 100–111, <https://doi.org/10.1016/j.carbon.2019.01.005>. N.Y.
- [32] J. Jiang, Q. Fan, S. Chou, Z. Guo, K. Konstantinov, H. Liu, J. Wang, Li₂S-based Li-ion sulfur batteries: progress and prospects, *Small* 17 (2021) 1903934, <https://doi.org/10.1002/sml.201903934>.
- [33] A. Bhargav, J. He, A. Gupta, A. Manthiram, Lithium–sulfur batteries: attaining the critical metrics, *Joule* 4 (2020) 285–291, <https://doi.org/10.1016/j.joule.2020.01.001>.
- [34] P. Li, J.Y. Hwang, Y.K. Sun, Nano/microstructured silicon–graphite composite anode for high-energy-density Li-ion battery, *ACS Nano* 13 (2019) 2624–2633, <https://doi.org/10.1021/acsnano.9b00169>.
- [35] F.T. Huld, S.Y. Lai, W.M. Tucho, R. Batmaz, I.T. Jensen, S. Lu, O.E. Eleri, A. Y. Kopusov, Z. Yu, F. Lou, Enabling increased delithiation rates in silicon-based anodes through alloying with phosphorus, *ChemistrySelect* 7 (2022) e202202857, <https://doi.org/10.1002/slct.202202857>.
- [36] N. Ding, J. Xu, Y.X. Yao, G. Wegner, X. Fang, C.H. Chen, I. Lieberwirth, Determination of the diffusion coefficient of lithium ions in nano-Si, *Solid State Ion* 180 (2009) 222–225, <https://doi.org/10.1016/j.ssi.2008.12.015>.
- [37] J. Ming, Z. Cao, W. Wahyudi, M. Li, P. Kumar, Y. Wu, J.Y. Hwang, M.N. Hedhili, L. Cavallo, Y.K. Sun, L.J. Li, New insights on graphite anode stability in rechargeable batteries: li ion coordination structures prevail over solid electrolyte interphases, *ACS Energy Lett.* 3 (2018) 335–340, <https://doi.org/10.1021/acscenergylett.7b01177>.
- [38] C. Li, T. Shi, H. Yoshitake, H. Wang, Improved performance in micron-sized silicon anodes by in situ polymerization of acrylic acid-based slurry, *J. Mater. Chem. A* 4 (2016) 16982–16991, <https://doi.org/10.1039/C6TA05650D>.
- [39] C. Li, X. Liu, L. Zhu, R. Huang, M. Zhao, L. Xu, Y. Qian, Conductive and polar titanium boride as a sulfur host for advanced lithium–sulfur batteries, *Chem. Mater.* 30 (2018) 6969–6977, <https://doi.org/10.1021/acs.chemmater.8b01352>.
- [40] X.B. Cheng, C. Yan, J.Q. Huang, P. Li, L. Zhu, L. Zhao, Y. Zhang, W. Zhu, S.T. Yang, Q. Zhang, The gap between long lifespan Li–S coin and pouch cells: the importance of lithium metal anode protection, *Energy Storage Mater.* 6 (2017) 18–25, <https://doi.org/10.1016/j.ensm.2016.09.003>.
- [41] L. Zhang, C. Zhao, Y. Lin, M. Wu, T. Zhao, A high-performance lithiated silicon–sulfur battery enabled by fluorinated ether electrolytes, *J. Mater. Chem. A* 9 (2021) 25426–25434, <https://doi.org/10.1039/D1TA05734K>.